A Brain Tumor Segmentation Framework Based on Outlier Detection Using One-Class Support Vector Machine

Ali Jalalifar, Hany Soliman, Mark Ruschin, Arjun Sahgal, and Ali Sadeghi-Naini, *Senior Member, IEEE*

***Abstract*— Accurate segmentation of brain tumors is a challenging task and also a crucial step in diagnosis and treatment planning for cancer patients. Magnetic resonance imaging (MRI) is the standard imaging modality for detection, characterization, treatment planning and outcome evaluation of brain tumors. MRI scans are usually acquired at multiple sessions before and after the treatment. An automatic segmentation framework is highly desirable to segment brain tumors in MR images as it streamlines the image-guided radiation therapy workflow considerably. Automatic segmentation of brain tumors also facilitates an incremental development of data-driven systems for therapy outcome prediction based on radiomics analysis. In this study, an outlier-detection-based segmentation framework is proposed to delineate brain tumors in magnetic resonance (MR) images automatically. The proposed method considers the tumor and edema pixels in an MR image as outliers compared to the pixels associated with the healthy tissue. The framework generates two outlier masks using independent one-class support vector machines that operate on post-contrast T1-weighted (T1w) and T2-weighted-fluid-attenuation-inversion-recovery (T2-FLAIR) images. The outlier masks are subsequently refined and fused using a number of morphological and logical operators to estimate a tumor mask for each image slice. The framework was constructed and evaluated using the MRI data acquired from 35 and 5 patients with brain metastasis, respectively. The obtained results demonstrated an average Dice similarity coefficient and Hausdorff distance of 0.84 ± 0.06 and 1.85 ± 0.48 mm, respectively, between the manual (ground truth) and automatic tumor contours, on the independent test set.**

I. Introduction

Unlike primary brain cancer which starts in the brain, brain metastasis is a malignancy that initiates in another part of the body and spread to the brain. Brain metastases are the most common brain tumors in adults, occurring in approximately %10 to %30 of cancer patients [1]. Planning for treatment of brain metastases depends on many factors including the origin of cancer, the symptoms, and number of metastases. External beam radiation therapy is a common treatment for brain metastasis which may include Whole-brain radiation therapy (WBRT) or Stereotactic radiation therapy (SRT). In some cases, surgical resection of tumor or systematic therapy is required alone or in combination with other treatments. Magnetic resonance imaging (MRI) is commonly used as part of the standard of care to detect, characterize, and manage the malignancies in brain. Accurate segmentation of brain tumors in magnetic resonance (MR) images is a challenging task and crucial in diagnosis, treatment planning and outcome evaluation after the treatment. In order to avoid the laborious task of manually segmenting tumors on several 2D planes of a 3D MRI acquired before and at multiple sessions after treatment, an automatic segmentation framework is highly desirable. The tumor area and its surrounding regions carry invaluable information for evaluating and potentially predicting the therapy outcome. Segmentation of these areas is time-consuming but a necessary step for evaluation and prediction of therapy outcome.

As mentioned above, an automatic brain tumor segmentation framework streamlines the radiation therapy evaluation workflow considerably. As part of standard follow-up evaluation and assessment, MRI scans are usually acquired at multiple sessions after the radiotherapy. The local response of the tumor to radiation therapy is determined based on the changes in physical measurements of the tumor [2]. Multiple follow-up scans for a large cohort of patients leave clinicians with many longitudinal images to segment manually, which is a tedious and time-consuming task. Therefore, automating the brain tumor segmentation process can accelerate the image-guided therapy evaluation workflow substantially.

The brain tumor area and its surrounding region (peritumoral area) can provide important information to predict the outcome of radiation therapy [3], [4]. More specifically, an automatic framework for brain tumor segmentation simplifies developing radiomics-based models of therapy response and outcome prediction [5]–[9]. Radiomics is defined as high-throughput extraction and analysis of a large number of features from medical images for specific diagnostic and/or prognostic applications using computational methods [5], [10]–[14]. To adapt radiomic models for personalized cancer therapeutics, tumor segmentation is required on different image modalities (e.g. pre- and post-contrast T1-weighted (T1w), T2-weighted and

*This research was supported by the Natural Sciences and Engineering Research Council (NSERC) of Canada, Terry Fox Foundation, and the Lotte and John Hecht Memorial Foundation.

A. Jalalifar is with the Department of Electrical Engineering and Computer Science, Lassonde School of Engineering, York University, Toronto, ON, Canada (e-mail: alijfar@yorku.ca).

H. Soliman, M. Ruschin, and A. Sahgal are with the Department of Radiation Oncology, Odette Cancer Centre, Sunnybrook Health Sciences Centre, Toronto, ON, Canada; also with the Department of Radiation Oncology, University of Toronto, Toronto, ON, Canada (e-mail:hany.soliman@sunnybrook.ca; mark.ruschin@sunnybrook.ca; arjun.sahgal@sunnybrook.ca).

A. Sadeghi-Naini is with the Department of Electrical Engineering and Computer Science, Lassonde School of Engineering York University, Toronto, ON, Canada; also with the Department of Radiation Oncology and Physical Sciences Platform, Odette Cancer Centre and Sunnybrook Research Institute, Sunnybrook Health Sciences Centre; also with the Department of Medical Biophysics, University of Toronto, Toronto, ON, Canada (e-mail: asn@yorku.ca, phone: 416-736-2100 x20590).

978-1-7281-1990-8/20/$31.00 ©2020 IEEE

T2-FLAIR images of brain) to extract relevant quantitative features. An automatic segmentation framework simplifies incremental development and modification of radiomics models for brain tumor management.

Automatic segmentation of brain tumors has been the focus of intense research in recent years and various algorithms have been proposed to perform this task. The proposed algorithms include threshold-based methods [15], region-based methods [16], segmentation techniques based on deformable models [17], and the methods based on deep-learning [18]. In this study, an automatic framework is proposed to segment brain tumors in gadolinium contrast-enhanced T1-weighted (T1w) and T2-weighted-fluid-attenuation-inversion-recovery (T2-FLAIR) images. In the proposed method, tumor and lesion (tumor + edema) regions in T1w and T2-FLAIR images, respectively, are considered as outlier tissues compared to the healthy tissues, i.e. white matter, gray matter, and the cerebrospinal fluid. Accordingly, the framework differentiates the tumor/lesion regions using an outlier detection technique called one-class support vector machine (OC-SVM). The T1w and T2-FLAIR images acquired for each patient are co-registered and small patches of the aligned images are independently used as the feature set for outlier detection. Finally, morphological and logical operations are applied to refine and fuse the segmentation masks for each slice. The framework was constructed and evaluated using the imaging data acquired from forty patients with metastatic brain tumors. The quantitative results indicated that the framework could segment the tumor with an average dice similarity coefficient of 0.84 ± 0.06 and Hausdorff distance of 1.85 ± 0.48 compared to the ground truth, on the independent test set.

II. Methods

A. Dataset

This study was conducted in accordance with institutional research ethics approval from Sunnybrook Health Sciences Centre (SHSC), Toronto, Canada. The imaging data were collected from 40 patients diagnosed with brain metastasis and planned for hypo-fractionated stereotactic radiation therapy (SRT). The dataset included the gadolinium contrast-enhanced T1w and T2-FLAIR images acquired before SRT for treatment planning. The in-plane image size and resolution were 512 × 512 and 0.5 × 0.5 mm, respectively, for both T1w and T2-FLAIR images. The slice thickness was 1.5 mm and 5 mm for T1w and T2-FLAIR images, respectively. The dataset also included the tumor contours for each patient, delineated by expert oncologists for treatment planning. These tumor contours were used as the ground truth for evaluation of the automatic segmentation framework. The data from 35 and 5 patients were used for training and testing the framework.

B. Segmentation Framework

The proposed segmentation framework considers tumor and edema pixels as statistical outliers within an image compared to the pixels associated with healthy brain tissues. The textural characteristics of tumor and edema regions are frequently different in comparison to the healthy tissues in T1w and T2-FLAIR images. Such characteristics can be captured in small patches of image that shows spatial variations in pixel intensity. As an initial step, the T2-FLAIR images were registered to their T1w image counterparts using an affine registration method with mutual information (MI) as the similarity metric [19]. The voxel spacing in the co-registered images was 0.5 × 0.5 × 1.5 mm. Subsequently, the skull was removed in both images using the BET (Brain Extraction Tool) software package [20]. The intensities in each image were normalized to have zero mean and unit standard deviation.

1) Outlier Mask Generation

In the outlier detection methodology applied in this study, only one class is defined for classification. This is in contrast with many other machine learning problems that usually include two or more classes. The target class (outlier pixels) was defined as the pixels within the tumor region in T1w image and the tumor and edema regions (lesion) in T2-FLAIR image. To classify each pixel, two patches with the size of 5×5 pixel were extracted from T1w and T2-FLAIR images in the corresponding slice with the target pixel in the center of the patch. The T1w and T2-FLAIR patches were fed to two independent outlier detection models. For training the models on T1w and T2-FLAIR images, only the patches associated with the tumor and lesion pixels were used, respectively. In other words, the target classes for the T1w and T2-FLAIR models were tumor and lesion, respectively. Here, the idea is to estimate the probability distribution of the samples associated with the tumor (lesion) regions in the MR images. The outlier detection model applies this probability distribution to predict whether a region (patch) in the T1w or T2-FLAIR image is part of the tumor (lesion) by calculating the distance of the patch to the estimated distribution.

To Estimate the probability distribution of the target class, OC-SVM was used [21]. support vector machines (SVMs) were introduced by Vapnik et. al. as a statistical classification method [22]. An SVM mainly performs classification by constructing hyperplanes in a multidimensional space that separate samples of different class labels. OC-SVMs are a natural extension of SVMs [21]. Basically, OC-SVMs estimate a distribution that encompasses most of the observations (target class), and consequently the points that lie far from it, with respect to a suitable metric, are not associated with the target class (tumor or lesion region in our case). OC-SVM separates all the data points from the origin (in feature space F) and maximizes the distance between the origin and the hyperplane that separates the points and origin. Finally, a binary function f is estimated which captures regions in the data space where the probability density of the target class is high.

We consider input data $x_1, x_2, \dots, x_l \in X$ where l is the number of samples. In our case x_i was a vector of normalized pixel intensities within a 5×5 patch extracted from the tumor region of the T1w image or the lesion region of the T2-FLARI image. Let Φ be a feature map, mapping space X to F, $X \to F$, i.e. a transformation into a dot product space F such that the dot product is calculated using:

$$k(x_i, x_j) = \left(\Phi(x_i).\Phi(x_j)\right), \quad (1)$$

This means that $k(x_i, x_j)$ is achieved by the dot product of $\Phi(x_i)$ and $\Phi(x_j)$. In our case, $k(x_i, x_j)$ is a Gaussian kernel and x_i and x_j are sample patches:

$$k(x_i, x_j) = e^{-\frac{||x_i{}^2 - x_j{}^2||}{2\sigma^2}} \quad (2)$$

where σ controls the width of the Gaussian kernel. The goal is to find function f that outputs the value $+1$ in a "small" region where data distribution of the target class exists, and -1 elsewhere. The solution is to map the data into the feature space corresponding to the kernel, and to separate them from the origin with maximum margin by calculating a separating hyperplane. Assigning a new input point *x* to the target class is determined by evaluating which side of the hyperplane (in the feature space) it belongs to. In a fashion similar to the two-class SVMs, the following quadratic program should be solved to separate the dataset form the origin,

$$\min_{\omega \epsilon F, \xi \epsilon R^l, \rho \epsilon R} \frac{1}{2}||\omega||^2 + \frac{1}{vl}\sum_i \xi_i - \rho, \quad (3)$$

Subject to:

$$(\omega . \Phi(x_i)) \geq \rho - \xi_i, \ \xi_i \geq 0 \quad (4)$$

where ω is the normal vector of the decision boundary hyperplane and ρ represents the threshold of function f, ξ_i is the slack variable which is penalized in the objective function. By introducing positive lagrangian multipliers α_i and β_i (for $i = 1,2,\dots,l$) to replace the inequality constraints in Eq. (4),

$$L(\omega, \xi, \rho, \alpha, \beta) = \frac{1}{2}\omega^T\omega + \frac{1}{vl}\sum_i \xi_i - \rho - \sum_i \beta_i \xi_i - \sum_i \alpha_i(\omega . \Phi(x_i) - \rho - \xi_i) \quad (5)$$

To minimize Eq. (5), its gradient with respect to ω, ρ, and ξ_i should be equal to zero, that is

$$\frac{\partial L}{\partial \omega} = \omega - \sum_i \alpha_i \Phi(x_i) = 0 \rightarrow \omega = \sum_i \alpha_i \Phi(x_i), \quad (6)$$

$$\frac{\partial L}{\partial \rho} = -1 + \sum_i \alpha_i = 0 \rightarrow \sum_i \alpha_i = 0, \quad (7)$$

$$\frac{\partial L}{\partial \xi_i} = \frac{1}{vl} + \alpha_i - \beta_i = 0 \rightarrow \frac{1}{vl} - \beta \leq \frac{1}{vl}. \quad (8)$$

Substituting Eq. (6) and (8) into Eq. (5) we obtain

$$\min_{\alpha} \frac{1}{2}\sum_{i,j} \alpha_i \alpha_j k(x_i, x_j) \ s.t. \ 0 \leq \alpha_i \leq \frac{1}{vl}, \ \sum_i \alpha_i = 1 \quad (9)$$

Once the optimal values a_i are obtained, the value of ρ can also be calculated via the equation

$$\rho = \sum_j \alpha_j k(x_j, x_i) \quad (10)$$

and the estimation function f is calculated as:

$$f(x) = sgn(\sum_i \alpha_i k(x_i, x) - \rho) \quad (11)$$

where *x* is the test patch.

2) Mask Fusion using Logical Operations

In this study, two independent OC-SVM models were trained for the co-registered T1w and T2-FLAIR images. For each new (test) patient, these models generated two masks (tumor, lesion) for each slice by classifying the overlapping 5×5 pixel patches of the entire T1w or T2-FLAIR image slice and assigning the estimated class to the center pixel of the patch.

These two masks were refined using dilation and erosion operators to reduce the noisy parts of the mask (scattered small white areas in the mask which are false-positives of OC-SVM) and also fill the holes in the mask within the tumor area. Subsequently, the refined outlier masks corresponding to the T1w and T2-FLAIR images were fused using a set of logical operators (described below) to obtain a final tumor mask for each slice of the co-registered MR images.

The idea behind using the T2-FLAIR image in the proposed tumor segmentation framework is based on the fact that edema is usually present around the tumor and it is generally clear and easy to detect on T2-FLAIR images. Hence, it can potentially be used to find an approximate location of the tumor to reduce the false-positive pixels in the segmentation mask. On this basis, the refined masks associated with the T1w (tumor) and T2-FLAIR (lesion) images were fused using an AND operation slice by slice. This operation potentially reduces the number of false-positive pixels in the fused mask, since to remain positive in the fused mask those pixels should have the value of 1 in both masks associated with the T1w and T2-FLAIR images. In the next step, an OR operation was applied over all slices in the fused mask to obtain a single-slice mask consisted of a large connected region and a few small scattered regions (the remaining false-positives). The center of the largest connected region obtained was used as an approximate position of the tumor to remove the false-positive areas in the tumor mask associated with the T1w image. For this purpose, an OR operation was applied over all slices of the tumor mask obtained from the T1w model to generate a single-slice mask consisted of a connected upper-bound area of the tumor and a number of scattered false-positive areas. We used the approximate position of the tumor obtained in the previous step to identify the connected region in this mask that shows an upper-bound area of the tumor. This connected region was maintained in the one-slice mask and all other regions (false-positives) were removed. In the last step, a final segmentation mask was generated for each image slice by ANDing each slice of the tumor mask (from the T1w model) with the obtained one-slice mask showing an upper-bound of the tumor area.

III. RESULTS

The segmentation results obtained using the T1w and T2-FLAIR images are shown in Fig. 1 for representative slices of the five tumors of the independent test set. This figure also presents the final segmentation masks generated by the framework as well as the ground truth masks. Qualitatively, the results obtained from the automatic segmentation framework agreed well with the ground truth. For example, patient one was a challenging case in which the tumor was located close to the ventricles. As observed in Fig. 1, the framework successfully outlined the tumor.

Table I presents the quantitative results of the automatic tumor segmentation in terms of Dice similarity coefficient and Hausdorff distance for the five patients (test set). The average Dice similarity coefficient between the manual and automatic tumor contours of these five patients ranged from

0.8 to 0.88. Table I also presents the average Hausdorff distance between the two contours throughout the all 2D slices of the tumor for each patient. The obtained average Hausdorff distance for 5 patients was 1.85 ± 0.48 mm.

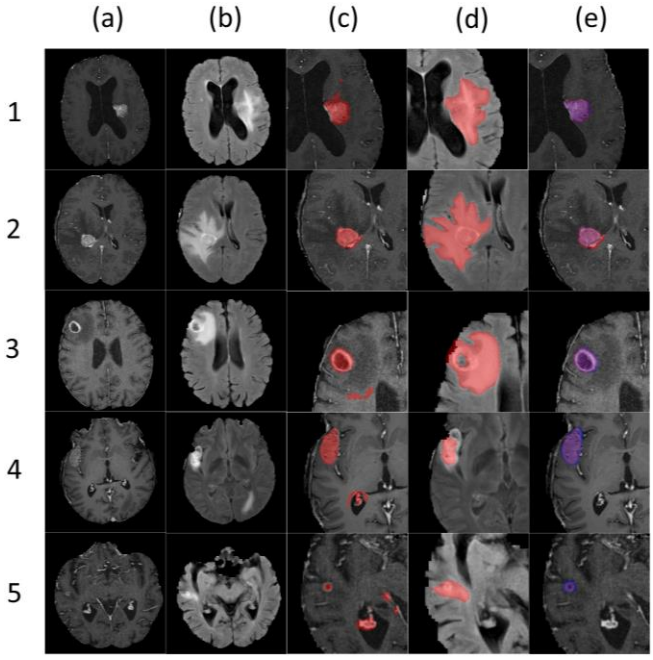

Figure 1. Segmentation results using OC-SVM: (a) the T1-w image, (b) T2-FLAIR image, (c) predicted tumor mask from the OC-SVM model trained on the T1w image, (d) predicted lesion mask from the model trained on T2-FLAIR image, (e) the ground-truth mask (blue), final segmentation mask (red) and the overlap region of the two masks (purple).

TABLE I. QUANTITATIVE RESULTS OF SEGMENTATION FOR FIVE PATIENTS

Patient #	Dice Similarity Coefficient	Average Hausdorff Distance
1	0.88 ± 0.06	1.34 ± 0.2 mm
2	0.84 ± 0.05	1.95 ± 0.4 mm
3	0.88 ± 0.03	1.24 ± 0.3 mm
4	0.80 ± 0.05	2.5 ± 0.7 mm
5	0.82 ± 0.06	2.2 ± 0.6 mm
Mean ± SD	0.84 ± 0.04	1.85 ± 0.48 mm

IV. DISCUSSION

In this study, a multi-block framework was proposed for automatic segmentation of brain tumors in standard MR images. The framework generated the tumor masks for each image slice based on anomaly detection using OC-SVM. The texture characteristics of tumor and edema regions are often different from healthy tissues in T1w and T2-FLAIR images. The framework applied such dissimilarity to detect the tumor and lesion regions automatically, and utilized morphological and logical operators to generate a fused tumor mask. Automating the process of brain tumor segmentation has several applications in clinic and leads to accelerating the process of radiation treatment planning and therapy outcome assessment. This work is a step forward towards automatic image-guided treatment planning, outcome evaluation, and development of data-driven predictive models of therapy outcomes for brain cancer patients. The results obtained in this study encourage further evaluation of the proposed method on a larger cohort of patients and comparison with other segmentation methods such as those based on deep learning.

REFERENCES

[1] I. T. Gavrilovic and J. B. Posner, "Brain metastases: epidemiology and pathophysiology," *J. Neurooncol.*, vol. 75, no. 1, pp. 5–14, 2005.

[2] N. U. Lin *et al.*, "Response assessment criteria for brain metastases: proposal from the RANO group," *Lancet Oncol.*, vol. 16, no. 6, pp. e270–e278, 2015.

[3] E. Karami *et al.*, "Quantitative MRI Biomarkers of Stereotactic Radiotherapy Outcome in Brain Metastasis.," *Sci. Rep.*, vol. 9, no. 1, p. 19830, 2019.

[4] E. Karami, M. Ruschin, H. Soliman, A. Sahgal, G. J. Stanisz, and A. Sadeghi-Naini, "An MR Radiomics Framework for Predicting the Outcome of Stereotactic Radiation Therapy in Brain Metastasis" in *41st Annual International Conference of the IEEE Engineering in Medicine and Biology Society (EMBC)*, 2019, pp. 1022–1025.

[5] A. Sadeghi-Naini *et al.*, "Conventional Frequency Ultrasonic Biomarkers of Cancer Treatment Response In Vivo," *Transl. Oncol.*, vol. 6, no. 3, pp. 234-IN2, 2013.

[6] A. Sadeghi-Naini *et al.*, "Imaging innovations for cancer therapy response monitoring," *Imaging Med.*, vol. 4, no. 3, pp. 311–327, 2012.

[7] H. J. W. L. Aerts *et al.*, "Decoding tumour phenotype by noninvasive imaging using a quantitative radiomics approach," *Nat. Commun.*, vol. 5, no. 1, p. 4006, 2014.

[8] Q. Li *et al.*, "A Fully-Automatic Multiparametric Radiomics Model: Towards Reproducible and Prognostic Imaging Signature for Prediction of Overall Survival in Glioblastoma Multiforme," *Sci. Rep.*, vol. 7, no. 1, p. 14331, 2017.

[9] A. Sadeghi-Naini *et al.*, "Early detection of chemotherapy-refractory patients by monitoring textural alterations in diffuse optical spectroscopic images," *Med. Phys.*, vol. 42, no. 11, pp. 6130–6146, 2015.

[10] R. J. Gillies, P. E. Kinahan, and H. Hricak, "Radiomics: Images Are More than Pictures, They Are Data," *Radiology*, vol. 278, no. 2, pp. 563–577, 2016.

[11] A. Sadeghi-Naini *et al.*, "Chemotherapy-Response Monitoring of Breast Cancer Patients Using Quantitative Ultrasound-Based Intra-Tumour Heterogeneities," *Sci. Rep.*, vol. 7, 10352, 2017.

[12] Q. T. Ostrom, C. H. Wright, and J. S. Barnholtz-Sloan, "Brain metastases: epidemiology.," *Handb. Clin. Neurol.*, vol. 149, pp. 27–42, 2018.

[13] H. Tadayyon *et al.*, "A priori Prediction of Neoadjuvant Chemotherapy Response and Survival in Breast Cancer Patients using Quantitative Ultrasound," *Sci. Rep.*, vol. 7, no. 1, p. 45733, 2017.

[14] A. Sadeghi-Naini *et al.*, "Quantitative Ultrasound Spectroscopic Imaging for Characterization of Disease Extent in Prostate Cancer Patients," *Transl. Oncol.*, vol. 8, no. 1, pp. 25–34, 2015.

[15] P. Gibbs, D. L. Buckley, S. J. Blackband, and A. Horsman, "Tumour volume determination from MR images by morphological segmentation," *Phys. Med. Biol.*, vol. 41, no. 11, pp. 2437–2446, 1996.

[16] A. Stadlbauer *et al.*, "Improved delineation of brain tumors: an automated method for segmentation based on pathologic changes of 1H-MRSI metabolites in gliomas," *Neuroimage*, vol. 23, no. 2, pp. 454–461, 2004.

[17] L. M. Fletcher-Heath, L. O. Hall, D. B. Goldgof, and F. R. Murtagh, "Automatic segmentation of non-enhancing brain tumors in magnetic resonance images," *Artif. Intell. Med.*, vol. 21, no. 1–3, pp. 43–63, 2001.

[18] M. Havaei *et al.*, "Brain tumor segmentation with Deep Neural Networks," *Med. Image Anal.*, vol. 35, pp. 18–31, 2017.

[19] D. L. G. Hill, P. G. Batchelor, M. Holden, and D. J. Hawkes, "Medical image registration," *Phys. Med. Biol.*, vol. 46, no. 3, pp. R1–R45, 2001.

[20] S. M. Smith, "Fast robust automated brain extraction," *Hum. Brain Mapp.*, vol. 17, no. 3, pp. 143–155, 2002.

[21] B. Schölkopf, R. C. Williamson, A. J. Smola, J. Shawe-Taylor, and J. C. Platt, "Support Vector Method for Novelty Detection.," *Adv. Neural Inf. Process. Syst.*, vol. 12, pp. 582–588, 1999.

[22] C. Cortes and V. Vapnik, "Support-vector networks," *Mach. Learn.*, vol. 20, no. 3, pp. 273–297, 1995.